JOURNAL OF AIRCRAFT
Vol. 39, No. 4, July–August 2002

Estimating the Low-Speed Downwash Angle on an Aft Tail

W. F. Phillips,* E. A. Anderson,† J. C. Jenkins,‡ and S. Sunouchi§
Utah State University, Logan, Utah 84322-4130

A closed-form analytic solution for the downwash induced on an aft tail by the main wing of an airplane is presented. This infinite series solution is based on Prandtl's classical lifting-line theory and accounts for the effects of wing planform shape, as well as tail position and vortex rollup. The results obtained from the present analysis reduce to the known solution for an elliptic wing. Results for a tapered wing are also presented. This infinite series solution applies only to a main wing with no sweep or dihedral. However, an approximate correction is presented, which can be used with some caution for swept wings. Results obtained from this analytic solution are compared with other methods and experimental data.

Nomenclature

B_n	=	coefficients in the infinite series
b	=	wingspan
b'	=	wingtip vortex spacing
C_{Lw}	=	wing lift coefficient
c_w	=	wing chord
R_{Aw}	=	wing aspect ratio
V_y	=	upwash velocity
V_∞	=	magnitude of the freestream velocity
x	=	axial coordinate
$\bar{x}$	=	dimensionless axial coordinate, $2x/b$
y	=	normal coordinate
$\bar{y}$	=	dimensionless normal coordinate, $2y/b$
z	=	spanwise coordinate
$\bar{z}$	=	dimensionless spanwise coordinate, $2z/b$
α	=	angle of attack
Γ	=	spanwise section circulation distribution
Γ_{wt}	=	wingtip vortex strength
γ_t	=	strength of shed vortex sheet per unit span
ε_d	=	downwash angle
θ	=	change of variables, spanwise coordinate
κ_b	=	wingtip vortex span factor
κ_p	=	tail position factor
κ_s	=	wing sweep factor
κ_v	=	wingtip vortex strength factor
Λ	=	quarter-chord wing sweep angle

Introduction

THE downwash induced on an aft tail by the main wing has a significant effect on the trim and static stability of an airplane. This downwash decreases the effective angle of attack for the horizontal tail and reduces its effectiveness in stabilizing the airplane. The downwash varies along the span of the horizontal tail and is affected by the planform shape of the wing, as well as the presence of the fuselage and nacelles. To obtain an accurate estimate for this interaction between the main wing and the tail, we must make use of computer simulations and/or wind-tunnel tests. Such methods are always employed in the later phases of the airplane design process. However, for the purpose of preliminary design, it is useful to have an approximate closed-form solution for estimating the downwash induced on the tail by the main wing. Such an approximate solution can be developed by assuming that the flow-field in the vicinity of the airplane is affected only by the main wing.

Prandtl's classical lifting-line theory[1,2] provides a closed-form solution for the spanwise distribution of vorticity generated by a finite wing. If the circulation about any section of the wing is $\Gamma(z)$, and the strength of the shed vortex sheet per unit span is $\gamma_t(z)$, as shown in Fig. 1, then Helmholtz's vortex theorem requires that the shed vorticity is related to the bound vorticity according to

$$\gamma_t(z) = -\frac{\mathrm{d}\Gamma}{\mathrm{d}z} \tag{1}$$

For the special case of an elliptic wing, Prandtl's lifting-line theory gives a very simple closed-form solution for the spanwise distribution of bound vorticity,

$$\Gamma(z) = \frac{2bV_\infty C_{Lw}}{\pi R_{Aw}}\sqrt{1-\left(\frac{2z}{b}\right)^2} \tag{2}$$

By the use of Eq. (2) in Eq. (1), the spanwise distribution of shed vorticity for an elliptic wing is

$$\gamma_t(z) = \frac{4V_\infty C_{Lw}}{\pi R_{Aw}}\frac{(2z/b)}{\sqrt{1-(2z/b)^2}} \tag{3}$$

When this vorticity distribution is used and the rollup of the shed vortex sheet ignored, it is readily shown that the downwash angle ε_d along the x axis far behind an elliptic wing, reduces to

$$\varepsilon_d(x,0,0) \underset{x\to\infty}{=} 2C_{Lw}/\pi R_{Aw} \tag{4}$$

The downwash angle computed from Eq. (4) has long been recommended as a first approximation for predicting the downwash on an aft tail (See, for example, Perkins and Hage[3] or Nelson[4]). This approximation has three shortcomings. First of all, it does not account for variations in the position of the tail relative to the main wing. In addition, it does not account for rollup of the shed vortex sheet. Finally, it does not account for variations in the planform shape of the main wing.

The rollup of the shed vortex sheet affects the downwash on an aft tail because it affects the proximity of this vorticity to the tail. The downwash angle computed from Eq. (4) is based on the assumption that the vortex filaments trailing downstream from the wing are all

Received 2 November 2001; presented as Paper 2002-0830 at the AIAA 40th Aerospace Sciences Meeting and Exhibit, Reno, NV, 14–17 January 2002; revision received 1 April 2002; accepted for publication 4 April 2002.

*Professor, Mechanical and Aerospace Engineering Department. Member AIAA.
†Assistant Professor, Mechanical and Aerospace Engineering Department. Senior Member AIAA.
‡Graduate Student, Mechanical and Aerospace Engineering Department. Member AIAA.
§Research Assistant, Mechanical and Aerospace Engineering Department.

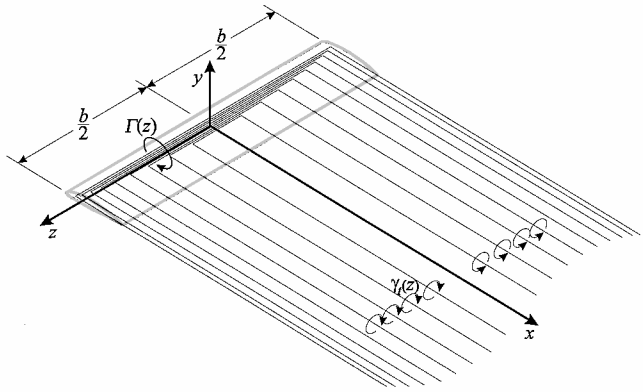

Fig. 1 Prandtl's model for the bound vorticity and the trailing vortex sheet generated by a finite wing.

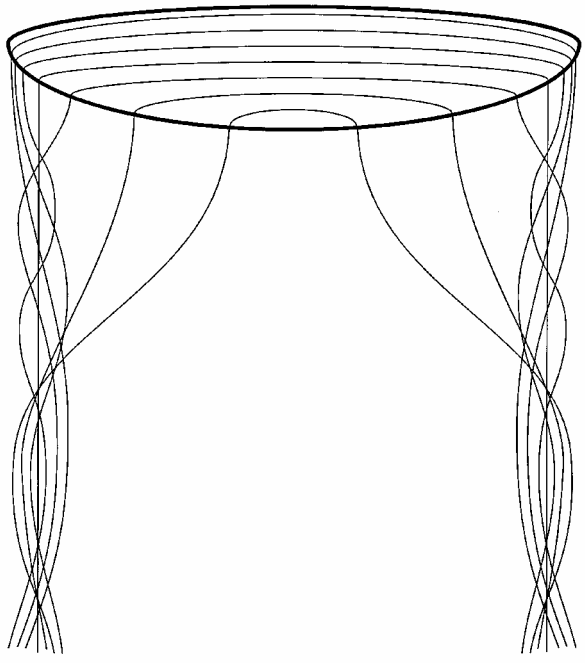

Fig. 2 Schematic of the vorticity rollup behind a finite wing with elliptic planform shape.

straight and parallel to the freestream flow, as shown in Fig. 1. In reality, the vorticity trailing from each side of the wing will roll up around an axis trailing somewhat inboard from the wingtip, as shown in Fig. 2. Within two to three chord lengths behind the wing, the vortex sheet becomes completely rolled up to form the wingtip vortices.[5–8]

Early experimental and theoretical investigations of wing downwash[9–14] eventually led to the development of a widely used empirical relation[15] for the downwash induced on an aft tail by a tapered wing. The result accounts for the effects of tail position, as well as variations in both aspect ratio and taper ratio of the main wing. This relation is still frequently used for preliminary calculations (for example, Roskam,[16] Etkin and Reid,[17] or Pamadi[18]). Recently, McCormick[19] proposed an analytical vortex model that accounts for the rollup of shed vorticity, as well as variations in the position of the tail relative to the main wing. However, this model is based on an elliptic main wing and does not account for other spanwise variations in chord length.

The present paper presents an analytical model for the downwash induced on an aft tail by a main wing having arbitrary spanwise variation in chord length. This model is based on the infinite series solution to Prandtl's classical lifting-line theory and, thus, can be directly applied only to a main wing with no sweep or dihedral. An approximate correction is also presented that can be used with some caution to account for the effects of sweep in the main wing.

Downwash Aft of an Unswept Wing

The well-known infinite series solution to Prandtl's classical lifting-line equation applies to a single finite wing with no sweep or dihedral, having an arbitrary spanwise variation in chord length. This solution is based on the change of variables

$$z = -\tfrac{1}{2}b\cos(\theta) \tag{5}$$

The variation in section circulation along the span of the wing, as predicted by this solution, is

$$\Gamma(\theta) = \frac{2bV_\infty C_{Lw}}{\pi R_{Aw}} \sum_{n=1}^{\infty} \frac{B_n}{B_1} \sin(n\theta) \tag{6}$$

For a complete presentation of Prandtl's lifting-line theory, see, for example, Anderson,[20] Katz and Plotkin,[21] McCormick,[22] or Bertin and Smith.[23]

Historically, the coefficients in this infinite series solution have usually been evaluated from collocation methods. Typically, the series is truncated to a finite number of terms, and the coefficients in the finite series are evaluated by requiring the lifting-line equation to be satisfied at a number of spanwise locations equal to the number of terms in the series. A very straightforward method was first presented by Glauert.[24] The most popular method, based on Gaussian quadrature, was originally presented by Multhopp.[25] Most recently, Rasmussen and Smith[26] have presented a more rigorous and rapidly converging method, based on a Fourier series expansion similar to that first used by Lotz[27] and Karamcheti.[28]

By the use of Eqs. (5) and (6) in Eq. (1), the spanwise variation of shed vorticity is

$$\gamma_t(\theta) = -\frac{4V_\infty C_{Lw}}{\pi R_{Aw}} \sum_{n=1}^{\infty} \frac{B_n}{B_1} \frac{n\cos(n\theta)}{\sin(\theta)} \tag{7}$$

The downwash distribution that is predicted directly from Eq. (7) is not accurate in the region behind the wing. This is because the development of Eq. (7) is based on the assumption that the vortex filaments trailing downstream from the wing are all straight and parallel to the freestream flow, as was shown in Fig. 1. In reality, the vorticity trailing from each side of the wing will roll up around an axis trailing slightly inboard from the wingtip, as is shown schematically for an elliptic wing in Fig. 2.

The rollup of the vortex sheet trailing behind each semispan of the wing can be viewed as a result of the vortex lifting law (see Saffman[29]). This vortex lifting law requires that, in any potential flow containing vortex filaments, a force is exerted on the surroundings that is proportional to the cross product of the local fluid velocity with the local filament vorticity. Because a free vortex filament cannot support a force, the cross product of the local fluid velocity with the local filament vorticity must be zero at every point along a free vortex filament. This means that all free vortex filaments must everywhere follow the streamlines of the flow. Thus, the free vortex filaments trailing behind each semispan of the wing will follow the streamlines and rollup about the center of vorticity shed from that semispan. Within a few chord lengths behind the wing, the vortex sheet becomes completely rolled up to form the wingtip vortices. This rollup has a significant effect on the downwash.

Each wingtip vortex is generated from the trailing vortex sheet produced by one-half of the wing. Therefore, a wingtip vortex, a few chord lengths or more behind the wing, can be approximated as a single vortex of strength Γ_{wt} which is given by

$$\Gamma_{wt} = \int_{z=0}^{b/2} \gamma_t(z)\,\mathrm{d}z \tag{8}$$

Using Eqs. (5) and (7) in Eq. (8) gives

$$\Gamma_{wt} = -\frac{2bV_\infty C_{Lw}}{\pi R_{Aw}} \sum_{n=1}^{\infty} \frac{B_n}{B_1} \int_{\theta=\pi/2}^{\pi} n\cos(n\theta)\,\mathrm{d}\theta \tag{9}$$

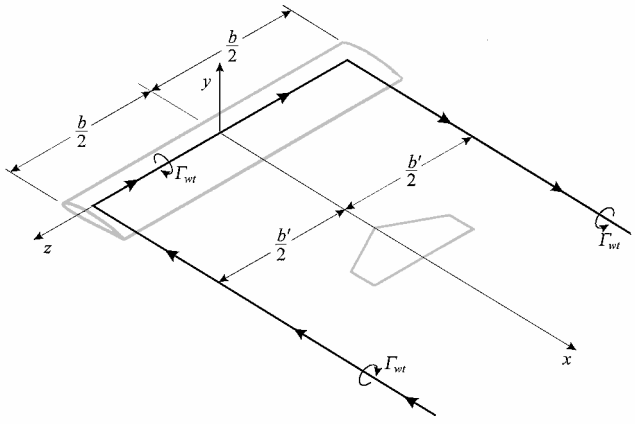

Fig. 3 Vortex model used for estimating the downwash a few chord lengths or more aft of an unswept wing.

Performing the indicated integration, we have

$$\Gamma_{\rm wt} = \frac{2bV_\infty C_{Lw}}{\pi R_{Aw}} \sum_{n=1}^{\infty} \frac{B_n}{B_1} \sin\left(\frac{n\pi}{2}\right) \tag{10}$$

When computing the downwash a few chord lengths or more downstream from a finite wing, we can approximate the rolled-up vortex sheet as a single horseshoe-shapedvortex filament of strength $\Gamma_{\rm wt}$, as shown in Fig. 3. The distance between the trailing vortices b' is less than the wingspan because the vortex sheet from each side of the wing rolls up around the center of vorticity, which is somewhat inboard from the wingtip. The horseshoe filament starts an infinite distance downstream from a point slightly inboard of the left wingtip, $(\infty, 0, b'/2)$, and runs upstream along the left wingtip vortex to the left wing, $(0, 0, b'/2)$. From there it runs across the wing quarter-chord to a point slightly inboard of the right wingtip, $(0, 0, -b'/2)$, and then downstream along the right wingtip vortex to infinity, $(\infty, 0, -b'/2)$. From the Biot–Savart law, the y-velocity component induced at any point (x, y, z) by this entire horseshoe vortex is

$$\begin{aligned} V_y(x, y, z) &= -\frac{\Gamma_{\rm wt}}{4\pi} \left\{ \frac{\frac{1}{2}b' - z}{y^2 + \left(\frac{1}{2}b' - z\right)^2} \left[1 + \frac{x}{\sqrt{x^2 + y^2 + \left(\frac{1}{2}b' - z\right)^2}} \right] \right. \\ &\quad + \frac{x}{x^2 + y^2} \left[\frac{\frac{1}{2}b' - z}{\sqrt{x^2 + y^2 + \left(\frac{1}{2}b' - z\right)^2}} \right. \\ &\quad \left. + \frac{\frac{1}{2}b' + z}{\sqrt{x^2 + y^2 + \left(\frac{1}{2}b' + z\right)^2}} \right] \\ &\quad \left. + \frac{\frac{1}{2}b' + z}{y^2 + \left(\frac{1}{2}b' + z\right)^2} \left[1 + \frac{x}{\sqrt{x^2 + y^2 + \left(\frac{1}{2}b' + z\right)^2}} \right] \right\} \end{aligned} \tag{11}$$

Because the vortex sheet shed from each semispan of the wing rolls up about the center of vorticity, we have

$$\frac{1}{2}b' = \frac{\int_{z=0}^{b/2} z\gamma_t(z)\,{\rm d}z}{\int_{z=0}^{b/2} \gamma_t(z)\,{\rm d}z} \tag{12}$$

Using Eq. (8) in Eq. (12) gives

$$b' = \frac{2}{\Gamma_{\rm wt}} \int_{z=0}^{b/2} z\gamma_t(z)\,{\rm d}z \tag{13}$$

When Eqs. (5), (7), and (10) are applied, this can be rewritten as

$$b' = b \left\{ \sum_{n=1}^{\infty} nB_n \int_{\theta=\pi/2}^{\pi} \cos(n\theta)\cos(\theta)\,{\rm d}\theta \Big/ \left[\sum_{n=1}^{\infty} B_n \sin\left(\frac{n\pi}{2}\right) \right] \right\} \tag{14}$$

The integration with respect to θ in Eq. (14) is readily carried out to give

$$\int_{\theta=\pi/2}^{\pi} \cos(n\theta)\cos(\theta)\,{\rm d}\theta = \begin{cases} \dfrac{\pi}{4}, & n = 1 \\ \dfrac{\cos(n\pi/2)}{(n^2-1)}, & n \neq 1 \end{cases} \tag{15}$$

Using Eq. (15) in Eq. (14) results in

$$b' = b \left\{ \left[\frac{\pi}{4} + \sum_{n=2}^{\infty} \frac{nB_n}{(n^2-1)B_1} \cos\left(\frac{n\pi}{2}\right) \right] \Big/ \left[1 + \sum_{n=2}^{\infty} \frac{B_n}{B_1} \sin\left(\frac{n\pi}{2}\right) \right] \right\} \tag{16}$$

Because the downwash is small compared to the freestream velocity, the downwash angle can be closely approximated as the downwash velocity divided by the freestream velocity. Thus, when Eqs. (10) and (16) are applied to Eq. (11), the downwash angle a few chord lengths or more downstream from an unswept wing is approximated as

$$\varepsilon_d(\bar{x}, \bar{y}, \bar{z}) \cong -V_y(\bar{x}, \bar{y}, \bar{z})/V_\infty = (\kappa_v \kappa_p/\kappa_b)(C_{Lw}/R_{Aw}) \tag{17}$$

where

$$\kappa_v = 1 + \sum_{n=2}^{\infty} \frac{B_n}{B_1} \sin\left(\frac{n\pi}{2}\right) \tag{18}$$

$$\kappa_b = \left\{ \left[\frac{\pi}{4} + \sum_{n=2}^{N} \frac{nB_n}{(n^2-1)B_1} \cos\left(\frac{n\pi}{2}\right) \right] \Big/ \left[1 + \sum_{n=2}^{N} \frac{B_n}{B_1} \sin\left(\frac{n\pi}{2}\right) \right] \right\} \tag{19}$$

$$\begin{aligned} \kappa_p(\bar{x}, \bar{y}, \bar{z}) &= \frac{1}{\pi^2} \left\{ \frac{\kappa_b(\kappa_b - \bar{z})}{\bar{y}^2 + (\kappa_b - \bar{z})^2} \left[1 + \frac{\bar{x}}{\sqrt{\bar{x}^2 + \bar{y}^2 + (\kappa_b - \bar{z})^2}} \right] \right. \\ &\quad + \frac{\kappa_b \bar{x}}{\bar{x}^2 + \bar{y}^2} \left[\frac{\kappa_b - \bar{z}}{\sqrt{\bar{x}^2 + \bar{y}^2 + (\kappa_b - \bar{z})^2}} \right. \\ &\quad \left. + \frac{\kappa_b + \bar{z}}{\sqrt{\bar{x}^2 + \bar{y}^2 + (\kappa_b + \bar{z})^2}} \right] \\ &\quad \left. + \frac{\kappa_b(\kappa_b + \bar{z})}{\bar{y}^2 + (\kappa_b + \bar{z})^2} \left[1 + \frac{\bar{x}}{\sqrt{\bar{x}^2 + \bar{y}^2 + (\kappa_b + \bar{z})^2}} \right] \right\} \end{aligned} \tag{20}$$

The dimensionless parameters κ_v and κ_b depend on the planform shape of the wing. For an elliptic wing, all of the coefficients B_n in the infinite series solution, except for the first, are zero. Using this with Eq. (18), we find that κ_v is 1.0 for an elliptic wing. Thus, from Eqs. (10) and (18), we see that the vortex strength factor κ_v is the ratio of the wingtip vortex strength to that generated by an elliptic wing having the same lift coefficient and aspect ratio. The vortex span factor κ_b is defined as the spacing between the wingtip vortices divided by the wingspan. Both κ_v and κ_b were determined analytically from the series solution to Prandtl's lifting-line equation. For an elliptic wing with no sweep, dihedral, or twist, κ_v is 1.0 and κ_b is $\pi/4$. For an unswept tapered wing with no dihedral or twist, κ_v and κ_b are related to the aspect ratio and taper ratio as is shown in Figs. 4 and 5.

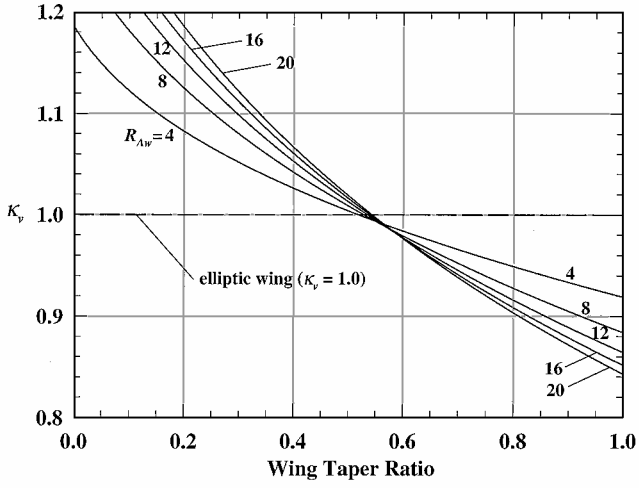

Fig. 4 Wingtip vortex strength factor as predicted from the series solution to Prandtl's lifting-line theory.

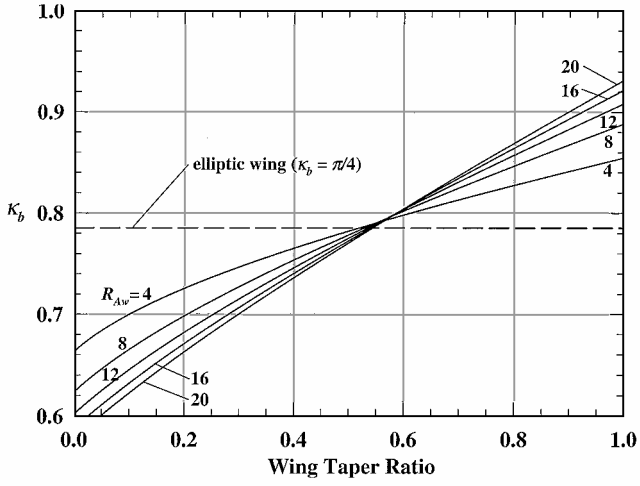

Fig. 5 Wingtip vortex span factor as predicted from the series solution to Prandtl's lifting-line theory.

The dimensionless parameter κ_p is a position factor that accounts for spatial variations in downwash. As a first approximation, the variation in downwash along the span of the horizontal tail is usually neglected. The downwash for the entire tail is typically taken to be that evaluated at the aerodynamic center. For a symmetric airplane, the aerodynamic center of the tail is in the plane of symmetry. The change in the downwash with respect to the spanwise coordinate is zero at the aircraft plane of symmetry. Furthermore, the span of the horizontal tail is usually small compared to that of the wing. Thus, the downwash is often fairly uniform over this span, and a reasonable first approximation for the downwash on an aft tail is found by setting the dimensionless spanwise coordinate $\bar{z}$ equal to zero in Eq. (20). This gives the relatively simple relation

$$\kappa_p(\bar{x}, \bar{y}, 0) = \frac{2\kappa_b^2}{\pi^2\left(\bar{y}^2 + \kappa_b^2\right)}\left[1 + \frac{\bar{x}\left(\bar{x}^2 + 2\bar{y}^2 + \kappa_b^2\right)}{(\bar{x}^2 + \bar{y}^2)\sqrt{\bar{x}^2 + \bar{y}^2 + \kappa_b^2}}\right] \tag{21}$$

The tail position factor κ_p depends on the planform shape of the wing and the position of the tail relative to the wing. The variation of κ_p with tail position in the plane of symmetry is shown in Fig. 6. The planform shape of the wing affects the value of κ_p only through its effect on κ_b. Thus, for a main wing with no sweep or dihedral, the value of κ_p in the plane of symmetry is a unique function of $\bar{x}/\kappa_b$ and $\bar{y}/\kappa_b$, as shown in Fig. 6.

Notice from Figs. 4 and 5 that the planform shape of the main wing has a very significant effect on the downwash induced on an aft tail. Similar results were observed empirically by Hoak,[15] but are not accounted for in the model proposed by McCormick.[19]

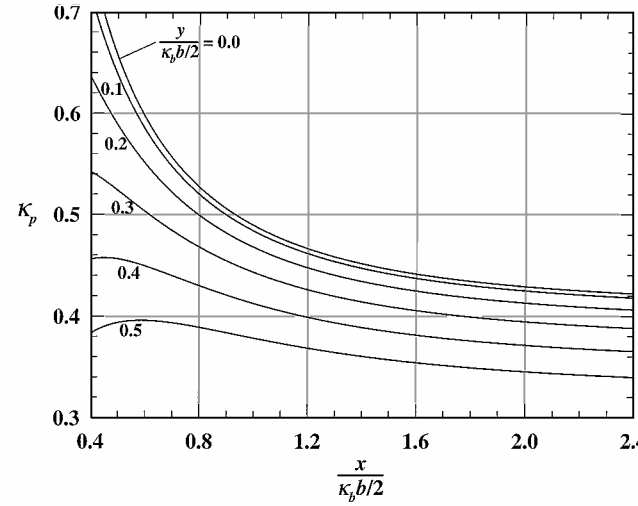

Fig. 6 Effect of tail position on the downwash angle in the plane of symmetry aft of an unswept wing.

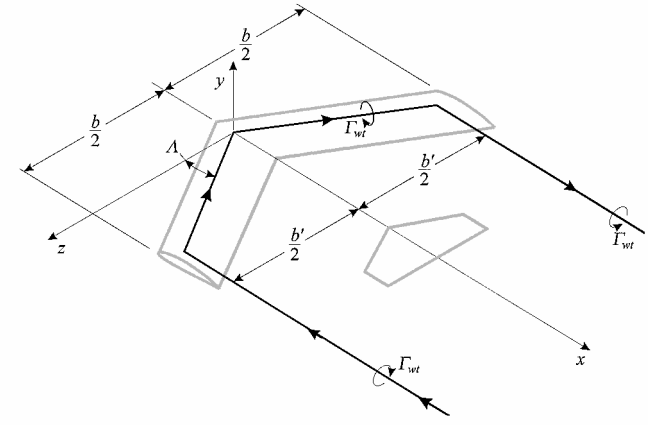

Fig. 7 Vortex model used for estimating the downwash a few chord lengths or more aft of a swept wing.

Approximate Correction for Swept Wings

Sweep in the main wing also has a significant effect on the downwash induced on an aft tail. Sweep affects this downwash in three ways. Because sweep changes the spanwise vorticity distribution on the wing, it changes the strength of the wingtip vortices for a given lift coefficient and aspect ratio. This same change in the vorticity distribution will also change the location of the center of vorticity in the vortex sheet shed from each semispan. Because each wingtip vortex rolls up around the center of vorticity from one side of the wing, wing sweep affects the spacing of the wingtip vortices. Because wing sweep affects both the strength and spacing of the wingtip vortices, sweep in the main wing will affect both κ_v and κ_b. More significantly, sweep in the main wing affects the downwash on an aft tail through a simple change in proximity of the wing surface to the tail. As the wing is swept back, the outboard portions of the wing are brought closer to the tail, as is shown in Fig. 7. This places the bound portion of the vortex system closer to the aft tail and, thus, changes the downwash induced on the tail.

Unfortunately, the series solution to Prandtl's classical lifting-line equation does not apply to a swept wing. No closed-form solution for the spanwise vorticity distribution on a swept wing has ever been obtained. In the absence of such a solution for this vorticity distribution, it is not possible to obtain a closed-form solution for the variation of κ_v and κ_b with sweep. Neglecting the effects of sweep on κ_v and κ_b is quite restrictive, and such results should be used with extreme caution for highly swept wings. Nevertheless, if we

are willing to neglect the effect of sweep on κ_v and κ_b, it is possible to obtain a closed-form approximation for the proximity effect that results from moving the bound vortex closer to the aft tail when the wing is swept back.

This approximation is based on the vortex model suggested by McCormick,[19] which is shown here in Fig. 7. With this model, the bound vorticity is approximated as two straight vortex line segments, one aligned with the quarter-chord of each semispan. Each wingtip vortex is modeled as a semi-infinite line vortex trailing from the wing at the center of shed vorticity. In reality, the direction of the trailing wingtip vortices is determined by the geometry of the airplane, the angle of attack, and the downward deflection of the vortex system, which is caused by the downwash that is induced on one vortex by the other. However, this level of sophistication is hardly justified when one considers the approximate nature of the other aspects of this vortex model. Instead, we shall simply assume that wingtip vortices trail downstream from the wing quarter-chord at the center of shed vorticity in a direction parallel to the x axis. In the development of Prandtl's classical theory, this same approximation was used.

With these approximations, the vorticity generated by a lifting swept wing is modeled as four straight vortex line segments, all of which fall in the x–z plane as shown in Fig. 7. By the application of the Biot–Savart law to this vortex system, in a manner similar to that used to obtain Eq. (11), the downwash in the aircraft plane of symmetry can be evaluated. If we continue with the assumption that the downwash is small compared to the freestream velocity, the result can be rearranged such that the downwash angle in the aircraft plane of symmetry a few chord lengths or more downstream from a swept wing is approximated as

$$\varepsilon_d(\bar{x}, \bar{y}, 0) \cong \frac{-V_y(\bar{x}, \bar{y}, 0)}{V_\infty} = \frac{\kappa_v \kappa_p \kappa_s}{\kappa_b} \frac{C_{Lw}}{R_{Aw}} \tag{22}$$

where

$$\kappa_s = \left[1 + \frac{\bar{x} - \bar{s}}{\bar{t}} + \frac{\bar{x}(\bar{r} + \bar{t})\left(\bar{t}_0^2 - \bar{x}^2\right)}{\bar{r}\bar{t}(\bar{r}\bar{t} + \bar{r}^2 - \bar{x}\,\bar{s})}\right] \Bigg/ \left[1 + \frac{\bar{x}\left(\bar{r}^2 + \bar{t}_0^2 - \bar{x}^2\right)}{\bar{r}^2 \bar{t}_0}\right] \tag{23}$$

$$\bar{r} \equiv \sqrt{\bar{x}^2 + \bar{y}^2} \tag{24}$$

$$\bar{s} \equiv \kappa_b \tan \Lambda \tag{25}$$

$$\bar{t} \equiv \sqrt{(\bar{x} - \bar{s})^2 + \bar{y}^2 + \kappa_b^2} \tag{26}$$

$$\bar{t}_0 \equiv \sqrt{\bar{x}^2 + \bar{y}^2 + \kappa_b^2} \tag{27}$$

The wing sweep factor κ_s depends on the planform shape of the wing and the position of the tail in addition to the quarter-chord sweep angle Λ. However, as was the case for κ_p, the planform shape of the wing affects the value of κ_s as predicted by Eq. (23) only through its effect on κ_b. Thus, in the aircraft plane of symmetry, κ_s is found to be a unique function of Λ, $\bar{x}/\kappa_b$, and $\bar{y}/\kappa_b$. The variation in κ_s with axial tail position is shown in Fig. 8, for several values of wing quarter-chord sweep and tail height. The results shown in Fig. 8, for the case $y = 0$, agree exactly with the results presented by McCormick[19] for the special case of an elliptic planform shape, that is, $\kappa_b = \pi/4$. However, McCormick states that the sweep correction "does not depend significantly on the tail height," and he suggests that the zero height solution may be used in general. Figure 8 does not support that statement.

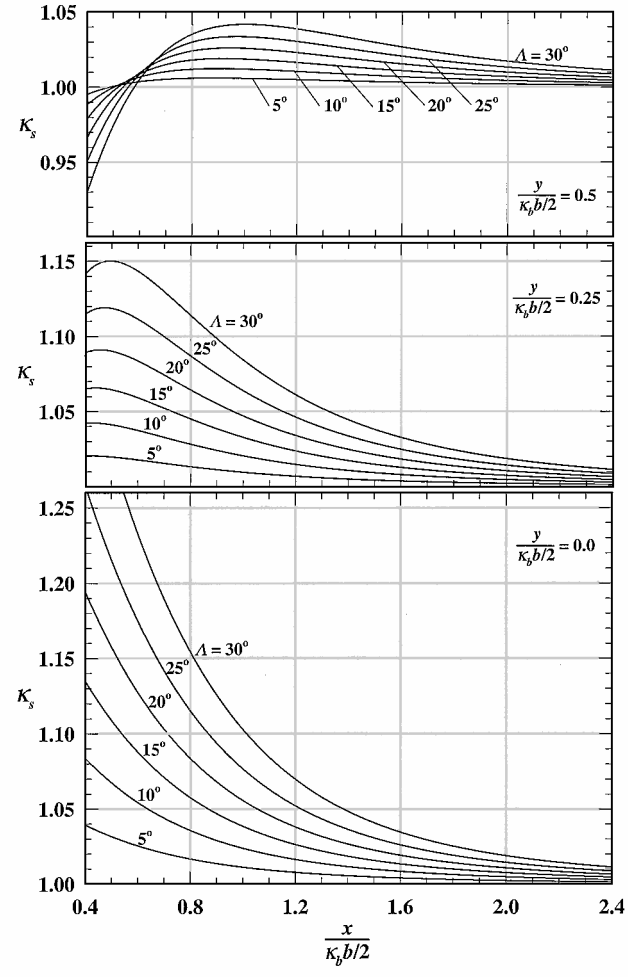

Fig. 8 Effect of wing sweep on the downwash in the plane of symmetry aft of the main wing.

Experimental Procedure and Uncertainty

As part of the process of validating the analytical solution presented here, experiments were conducted in the low-speed wind tunnel at Utah State University's Aerodynamics Research Laboratory. The tunnel is an in-draft type with a 1.2×1.2 m test section and an inlet contraction ratio of 9:1. A 200-hp three-phase electric motor with a computer controlled variable frequency drive rotates the 1.83-m-diam variable pitch propeller. Maximum speed capability of the tunnel is 50 m/s with a corresponding turbulence intensity of less that 0.5%. Experiments were performed at a tunnel velocity of 25 m/s corresponding to a chord Reynolds number of 1.7×10^5.

A rectangular planform NACA 0015 wing with rounded end caps was used in this study. The wing chord of 12.7 cm and span of 66.0 cm gave an aspect ratio of 5.2. The relative positioning accuracy of wing incidence was ± 0.1 deg. Note that the accuracy of the absolute incidence angle is not reported because the results are presented in terms of change in downwash angle with respect to changes in wing incidence, which is independent of the absolute incidence angle. The wing was mounted at the vertical center of the test section on two vertical struts extending from a splitter plate located 10 cm above the tunnel floor. The struts were attached to the wing at quarter-chord positions with a symmetric spanwise separation of 18 cm.

Downwash angle and velocity measurements were obtained using a TSI 1240-20 x-type hot-film probe and a TSI IFA300 constant temperature anemometer system. The mean velocity results presented in this study are based on an average of 2^{14} samples per data point acquired at a sample rate of 2000 Hz for a total sample period of 8.192 s. The sample period was defined by the minimum period beyond which the statistical quantities remain constant and repeatable. Calibration of the hot-wire probes was accomplished with a TSI Model 1129 automatic air velocity calibrator using 11 points to cover a velocity range of 0–30 m/s. The mean standard errors of the velocity calibration are as follows: less than 2% for velocities between 0 and 1 m/s, less than 1% for velocities between 1 and 8 m/s, and less than 0.5% for velocities greater than 8 m/s. The probe was calibrated over a pitch angle range of ± 30 deg using 5-deg increments at a velocity of 23.0 m/s. Several recalibrations

were required to maintain the accuracy of the velocity results and they occurred at least within 24 h of any test results reported in this study. The freestream dynamic pressure was determined from a pitot-static probe located upstream of the model. Dynamic pressure was converted to tunnel velocity using real-time ambient pressure and temperature measurements.

The streamwise origin of the coordinate system is located at the aerodynamic center of the wing section, whereas the origin of the transverse axis is defined by the location of the trailing vortex at the streamwise measurement location. Hence, the transverse origin is a function of wing incidence. The transverse origin at each streamwise measurement location was determined by x-sensor traverses near the spanwise positions of the wingtips.

Downwash velocity components were obtained using traverses from $2y/b = 0.00$ to 0.46 with an increment of 0.019 at three spanwise locations, $2z/b = -0.077, 0.0$, and 0.077. The reported results represent a spatial average over the spanwise measurement range. The area based solid blockage of the wind tunnel, including support struts, varied from 2.5 to 3.1% over the tested angle-of-attack range of 2.0–8.0 deg. Because the solid blockage was small and varied little over the angle-of-attack range covered, the reported downwash results were not corrected for tunnel wall interference, and tunnel upwash corrections were not applied. This is justified because the results are presented in terms of a relative change in downwash angle with respect to change in wing incidence at a fixed measurement location. Because there was very little variation in solid blockage over the angle-of-attack range covered, any upwash due to imperfections in the tunnel walls should not change significantly with wing angle of attack. Thus, any flow angularity caused by the tunnel walls was assumed to be independent of wing incidence. Although such tunnel upwash has a significant effect on the magnitude of the downwash angle measured aft of the wing, it should not significantly affect the measured downwash gradient, which is determined from the change in downwash angle measured at different angles of attack.

Results

To validate the spatial variation in downwash predicted by the proposed analytical solution, results obtained from this model were compared with the experimental wind-tunnel data. The solution was also compared with the empirical correlation of Hoak[15] and the analytical method proposed by McCormick.[19] These comparisons are shown in Figs. 9–13 for the unswept rectangular wing that was described in the preceding section. The data collected in the present study were restricted to a single wing of aspect ratio 5.2 and taper ratio 1.0. Although this allows us to examine the accuracy of the proposed method for predicting the spatial variation in downwash, little can be inferred from these data about the ability of the model to predict the effects of wing planform.

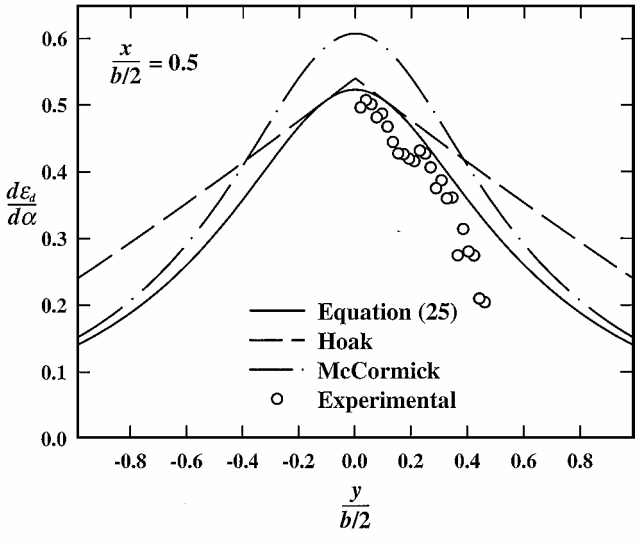

Fig. 9 Downwash in the plane of symmetry aft of a rectangular wing of aspect ratio 5.2, at $\bar{x} = 0.5$.

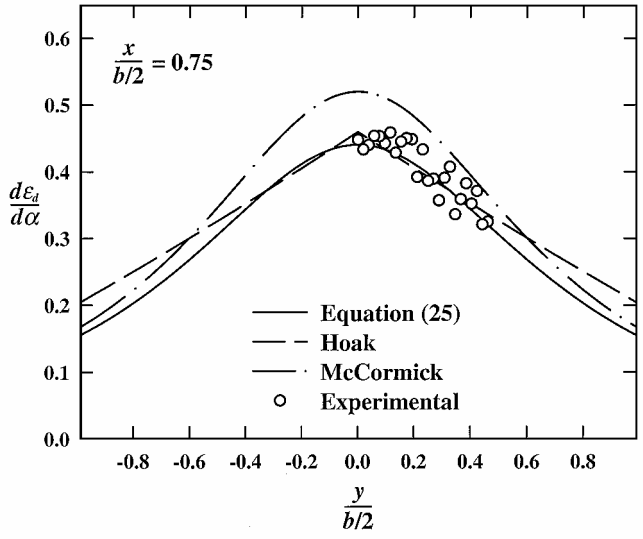

Fig. 10 Downwash in the plane of symmetry aft of a rectangular wing of aspect ratio 5.2, at $\bar{x} = 0.75$.

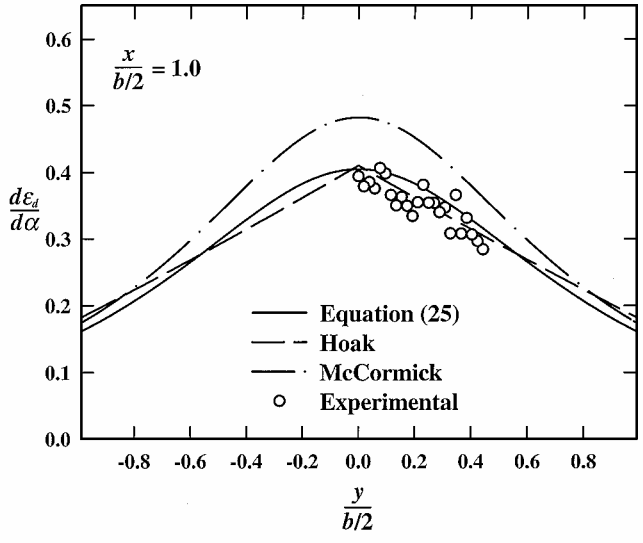

Fig. 11 Downwash in the plane of symmetry aft of a rectangular wing of aspect ratio 5.2, at $\bar{x} = 1.0$.

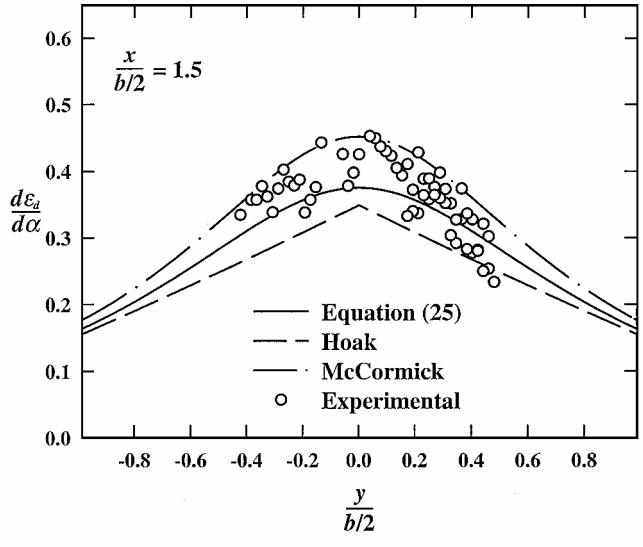

Fig. 12 Downwash in the plane of symmetry aft of a rectangular wing of aspect ratio 5.2, at $\bar{x} = 1.5$.

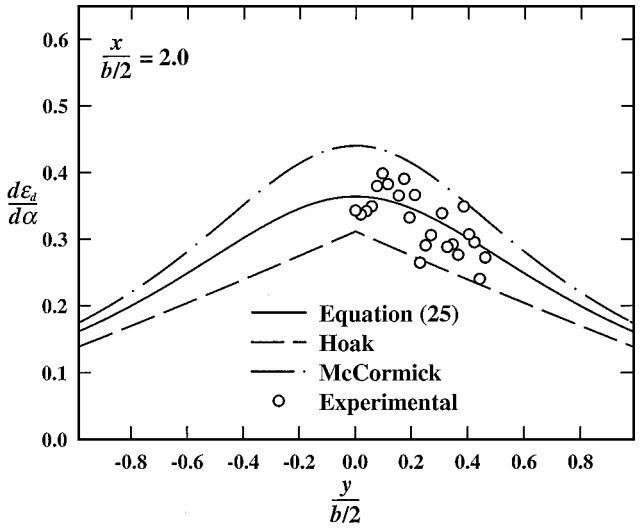

Fig. 13 Downwash in the plane of symmetry aft of a rectangular wing of aspect ratio 5.2, at $\bar{x} = 2.0$.

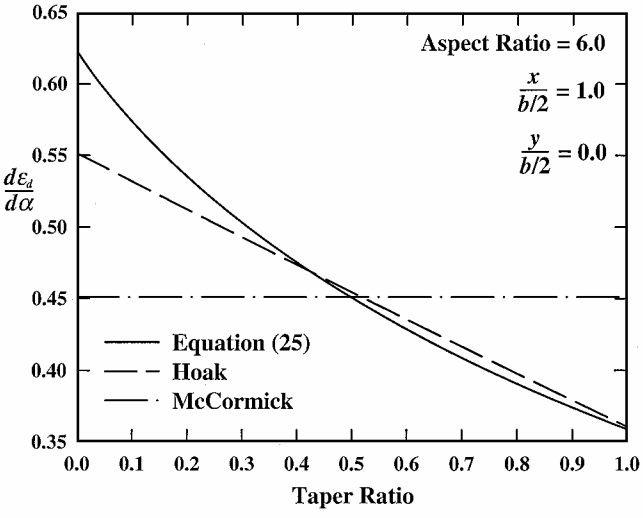

Fig. 14 Effects of taper ratio on the downwash in the plane of symmetry aft of a tapered wing.

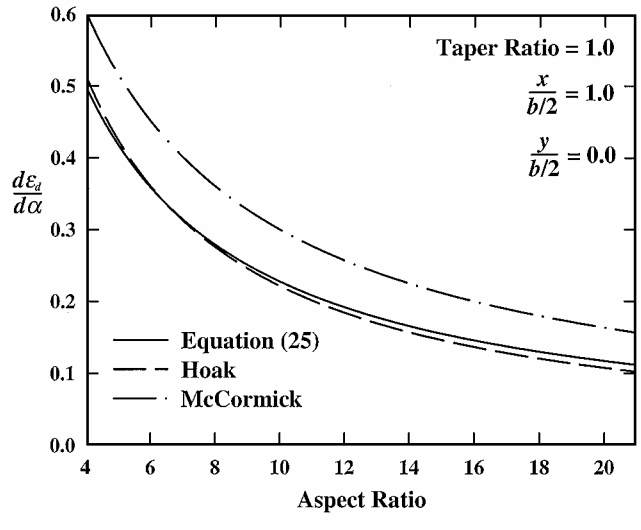

Fig. 15 Effects of aspect ratio on the downwash in the plane of symmetry aft of a rectangular wing.

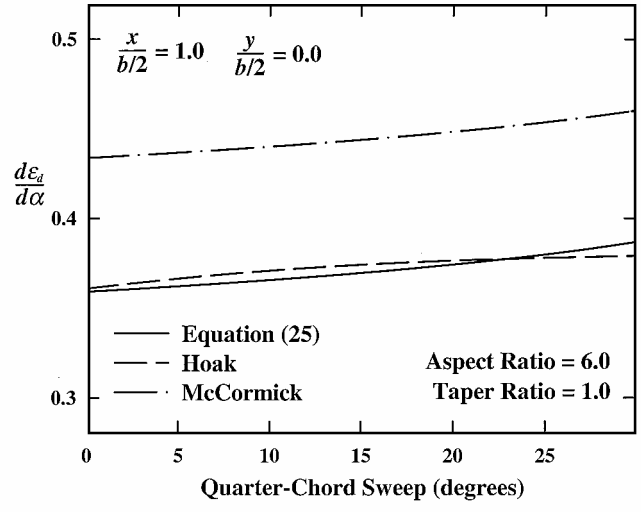

Fig. 16 Effects of sweep on the downwash in the plane of symmetry aft of a wing with no taper.

To examine how well the present model predicts the effects of wing planform shape, the proposed solution was compared with the empirical correlation of Hoak.[15] Because the empirical correlation was taken from experimental data, it should be reasonably accurate, at least over the range of parameters for which the correlation was obtained. Figure 14 shows a comparison between the empirical correlation and the present analytical solution for taper ratios from 0.0 to 1.0. This comparison is based on the downwash one semispan directly aft of the center of a wing with aspect ratio 6.0. The result predicted by the analytical method of McCormick[19] is also shown in Fig. 14. Similar comparisons showing the effect of aspect ratio and sweep are presented in Figs. 15 and 16.

In the region very close behind the wing, both the present analytical solution and the empirical correlation[15] begin to deviate from the experimental data obtained in the current study. Because the empirical correlation was developed for prediction of the downwash gradient on an aft tail, it is not likely that any attempt was made to correlate data that were taken very close behind the wing. The deviation between the experimental data taken close to the wing and the present analytical model is likely a result of the approximate manner in which lifting-line theory handles the bound vorticity. The present analytical model neglects the streamwise distance required for the shed vorticity to roll up and form the wingtip vortices. The model assumes a single wingtip vortex shed from the wing quarter-chord as shown in Fig. 3. This model should not be expected to give accurate results for locations very close to the wing, and it is tempting to blame the errors that occur close to the wing on our failure to account for the transition region of partial vortex rollup. However, as will be demonstrated, this is not the case.

To examine how vortex rollup affects the downwash angle aft of the wing, we can compare results computed from the present model with those obtained from the classical lifting-line model, which neglects all vortex rollup, as shown in Fig. 1. From the classical lifting-line solution, the downwash angle induced by the unrolled vortex sheet at an arbitrary point in space is given by

$$\varepsilon_d(\bar{x}, \bar{y}, \bar{z}) = \frac{C_{Lw}}{R_{Aw}} \sum_{n=1}^{N} \frac{B_n}{\pi^2 B_1} \int_{\theta=0}^{\pi} \left\{ \frac{n \cos(n\theta)[\bar{z} + \cos(\theta)]}{\bar{y}^2 + [\bar{z} + \cos(\theta)]^2} \right.$$

$$+ \frac{n\bar{x} \cos(n\theta)[\bar{z} + \cos(\theta)]}{\{\bar{y}^2 + [\bar{z} + \cos(\theta)]^2\}\{\bar{x}^2 + \bar{y}^2 + [\bar{z} + \cos(\theta)]^2\}^{\frac{1}{2}}}$$

$$\left. + \frac{\bar{x} \sin(n\theta) \sin(\theta)}{\{\bar{x}^2 + \bar{y}^2 + [\bar{z} + \cos(\theta)]^2\}^{\frac{3}{2}}} \right\} d\theta \qquad (28)$$

The integration required to evaluate this expression for an arbitrary point in space is quite complex and will not be addressed here. However, for large distances directly downstream from the spanwise

midpoint of the wing, integration of Eq. (28) yields a very simple result for the far-field downwash with no vortex rollup,

$$\varepsilon_d(\infty, 0, 0) = \frac{2}{\pi}\left[1 + \sum_{n=2}^{N} \frac{n B_n}{B_1} \sin\left(\frac{n\pi}{2}\right)\right]\frac{C_{Lw}}{R_{Aw}} \tag{29}$$

From Eqs. (17) and (20), the far-field downwash including vortex rollup is given by

$$\varepsilon_d(\infty, 0, 0) = \left(4\kappa_v / \pi^2 \kappa_b\right)(C_{Lw}/R_{Aw}) \tag{30}$$

For the special case of an elliptic wing, Eq. (29) reduces to Eq. (4) and the far-field downwash with no vortex rollup would be $\varepsilon_d(\infty, 0, 0)R_{Aw}/C_{Lw} = 2/\pi$. From Eq. (30), the far-field downwash for an elliptic wing including vortex rollup is $\varepsilon_d(\infty, 0, 0)R_{Aw}/C_{Lw} = 16/\pi^3$. Similarly, for a rectangular wing of aspect ratio 6.0, neglecting vortex rollup gives $\varepsilon_d(\infty, 0, 0)R_{Aw}/C_{Lw} = 0.464$, and including vortex rollup yields $\varepsilon_d(\infty, 0, 0)R_{Aw}/C_{Lw} = 0.417$. For a tapered wing of aspect ratio 6.0 and taper ratio 0.5, Eq. (29) results in $\varepsilon_d(\infty, 0, 0)R_{Aw}/C_{Lw} = 0.743$ and Eq. (30) predicts $\varepsilon_d(\infty, 0, 0)R_{Aw}/C_{Lw} = 0.523$. Thus, we see that complete vortex rollup reduces the far-field downwash by 10–30%, depending on the planform shape of the wing. In the region close behind the wing, we would expect the partial vortex rollup to reduce the downwash somewhat, but the reduction should be less than that predicted under the assumption of complete vortex rollup. As a result, the rollup approximation used in the present analytical model tends to underpredict the downwash induced by the trailing vorticity in the region close behind the wing. However, the approximate manner in which the present model handles the bound vorticity tends to overpredict the downwash induced by the bound vorticity in the region close behind the wing. Thus, the effects of these two approximations tend to cancel, and the model agrees closely with both the empirical correlation of Hoak[15] and the present experimental data for tail positions as close as two chord lengths aft of the wing. For example, the comparison shown in Fig. 10 corresponds to $x/c_w = 1.95$. In the region less than two chord lengths aft of the wing, the downwash is affected more by the bound vorticity than by the trailing vorticity, and the present model will overpredict the downwash gradient.

For locations far aft of the wing, the empirical correlation[15] again shows some deviation from the current wind-tunnel data, whereas the proposed analytical model appears to better represent the experimental mean in this region. Here again, because such locations are outside the region where an aft tail would typically be encountered, it is not likely that the empirical correlation[15] is based on data that were taken far aft of the wing. On the other hand, the lifting-line approximation used in the present analytical model should be expected to improve with increasing distance from the wing.

In Fig. 14, it is seen that the empirical correlation[15] and the proposed analytical model agree very closely for taper ratios in the range from about 0.3 to 1.0. For taper ratios less than 0.3, the analytical model begins to deviate significantly from the empirical correlation.[15] Because taper ratios less than 0.3 are not typically used for subsonic aircraft, it is very doubtful that wings of such severe taper were used in the development of this empirical correlation.[15] In any case, taper ratios less than 0.3 are of no practical importance for low-speed aircraft. Because the analytical model of McCormick[19] is based on an elliptic wing planform, Fig. 14 shows no variation in this result with taper ratio.

When the effects of aspect ratio are examined, Fig. 15 shows almost perfect agreement between the proposed analytical model and the empirical correlation,[15] for aspect ratios between 4 and 20. Because the analytical model presented here is based on lifting-line theory, it should not be expected to give accurate results for aspect ratios less than about four. The analytical model proposed by McCormick[19] also correctly predicts the effects of aspect ratio. The discrepancy that is seen in Fig. 15 for this model is the result of wing planform, not aspect ratio.

As can be seen in Fig. 16, the effect of sweep is not large, over the range of sweep typically encountered in subsonic airplanes. Furthermore, agreement between the empirical correlation[15] and the proposed analytical model appears to be reasonably good for sweep angles less than 30 deg.

Conclusions

From the results presented here, it can be seen that the proposed analytical model agrees very closely with both the empirical correlation of Hoak and with the present experimental data, over the range of spatial coordinates where an aft tail might typically be located. This should give some confidence in the model, at least for the prediction of downwash on an aft tail.

Because the analytical model proposed here agrees very closely with the empirical correlation of Hoak, a question may naturally arise in the mind of the reader. That is, what advantage does the present analytical model provide? The answer is quite simple. The analytical model proposed by McCormick is valid only for an elliptic wing and the empirical correlation of Hoak applies only to a tapered wing with no geometric or aerodynamic twist. The analytical model proposed here, on the other hand, can be used for a wing with completely arbitrary spanwise variations in chord length, section geometric angle of attack, and section zero-lift angle of attack. For example, the present model can be used to predict the effects of double taper, washout, and other spanwise variations in the wing section properties. Furthermore, the computations required for this model are simple enough to be carried out on a modern programmable calculator.

References

[1]Prandtl, L., "Tragflügel Theorie," *Nachricten von der Gesellschaft der Wissenschaften zu Göttingen*, Ges-chäeftliche Mitteilungen, Klasse, Germany, 1918, pp. 451–477.

[2]Prandtl, L., "Applications of Modern Hydrodynamics to Aeronautics," NACA TR-116, June 1921.

[3]Perkins, C. D., and Hage, R. E., "Tail Contribution," *Airplane Performance Stability and Control*, Wiley, New York, 1949, pp. 219–223.

[4]Nelson, R. C., "Tail Contribution-Aft Tail," *Flight Stability and Automatic Control*, 2nd ed., McGraw–Hill, New York, 1998, pp. 47–52.

[5]McCormick, B. W., Tangler, T. L., and Sherrieb, H. E., "Structure of Trailing Vortices," *Journal of Aircraft*, Vol. 5, No. 3, 1968, pp. 260–267.

[6]Green, S. I., and Acosta, A. J., "Unsteady Flow in Trailing Vortices," *Journal of Fluid Mechanics*, Vol. 227, 1991, pp. 107–134.

[7]Devenport, W. J., Rife, M. C., Liapis, S. I., and Follin, G. J., "The Structure and Development of the Wing-Tip Vortex," *Journal of Fluid Mechanics*, Vol. 312, 1996, pp. 67–106.

[8]Ramaprian, B. R., and Zheng, Y., "Measurements in Rollup Region of the Tip Vortex from a Rectangular Wing," *AIAA Journal*, Vol. 35, No. 12, 1997, pp. 1837–1843.

[9]Diehl, W. S., "The Determination of Downwash," NACA TN-42, Jan. 1921.

[10]Munk, M. M., and Cairo, G., "Downwash of Airplane Wings," NACA TN-124, Jan. 1923.

[11]Silverstein, A., and Katzoff, S., "Design Charts for Predicting Downwash Angles and Wake Characteristics Behind Plain and Flapped Wings," NACA TR-648, 1939.

[12]Silverstein, A., Katzoff, S., and Bullivant, W. K., "Downwash and Wake Behind Plain and Flapped Airfoils," NACA TR-651, 1939.

[13]Hoggard, H. P., and Hagerman, J. R., "Downwash and Wake Behind Untapered Wings of Various Aspect Ratios and Angle of Sweep," NACA TN-1703, 1948.

[14]Diederich, F. W., "Charts and Tables for use in Calculations of Downwash of Wings of Arbitrary Plan Form," NACA TN-2353, May 1951.

[15]Hoak, D. E., "USAF Stability and Control Datcom," U.S. Air Force Wright Aeronautical Labs., AFWAL-TR-83-3048, Wright–Patterson AFB, OH, Oct. 1960 (revised 1978).

[16]Roskam, J., "Lift and Pitching Moment Prediction Methods," *Airplane Design Part VI: Preliminary Calculations of Aerodynamic, Thrust and Power Characteristics*, DAR Corp., Lawrence, KS, 1990, pp. 213–354.

[17]Etkin, B., and Reid, L. D., "Downwash," *Dynamics of Flight: Stability and Control*, 3rd ed., Wiley, New York, 1996, pp. 332–334.

[18]Pamadi, B. N., "Tail Contribution," *Performance, Stability, Dynamics, and Control of Airplanes*, AIAA, Reston, VA, 1998, pp. 194–198.

[19]McCormick, B. W., "Downwash Angle," *Aerodynamics, Aeronautics, and Flight Mechanics*, 2nd ed., Wiley, New York, 1995, pp. 479–482.

[20]Anderson, J. D., "Incompressible Flow over Finite Wings: Prandtl's Classical Lifting-Line Theory," *Fundamentals of Aerodynamics*, 3rd ed., McGraw–Hill, New York, 1991, pp. 360–387.

[21]Katz, J., and Plotkin, A., "Finite Wing: The Lifting-Line Model," *Low-Speed Aerodynamics, from Wing Theory to Panel Methods*, McGraw–Hill, New York, 1991, pp. 193–212.

[22]McCormick, B. W., "The Lifting Line Model," *Aerodynamics, Aeronautics, and Flight Mechanics*, 2nd ed., Wiley, New York, 1995, pp. 112–119.

[23]Bertin, J. J., and Smith, M. L., "Incompressible Flow About Wings of Finite Span," *Aerodynamics for Engineers*, 3rd ed., Prentice–Hall, Upper Saddle River, NJ, 1998, pp. 261–336.

[24]Glauert, H., *The Elements of Aerofoil and Airscrew Theory*, 2nd ed., Cambridge Univ. Press, Cambridge, England, U.K., 1959, pp. 142–145.

[25]Multhopp, H., "Die Berechnung der Auftriebs Verteilung von Tragflugeln," *Luftfahrtforschung*, Vol. 15, No. 14, 1938, pp. 153–169.

[26]Rasmussen, M. L., and Smith, D. E., "Lifting-Line Theory for Arbitrarily Shaped Wings," *Journal of Aircraft*, Vol. 36, No. 2, 1999, pp. 340–348.

[27]Lotz, I., "Berechnung der Auftriebsverteilung Beliebig Geformter Flugel," *Zeitschrift für Flugtechnik und Motorluftschiffahrt*, Vol. 22, No. 7, 1931, pp. 189–195.

[28]Karamcheti, K., "Elements of Finite Wing Theory," *Ideal-Fluid Aerodynamics*, Wiley, New York, 1966, pp. 535–567.

[29]Saffman, P. G., "Vortex Force and Bound Vorticity," *Vortex Dynamics*, Cambridge Univ. Press, Cambridge, England, U.K., 1992, pp. 46–48.